INSTITUTE OF PHYSICS PUBLISHING JOURNAL OF PHYSICS B: ATOMIC, MOLECULAR AND OPTICAL PHYSICS

J. Phys. B: At. Mol. Opt. Phys. **37** (2004) 471–483 PII: S0953-4075(04)69605-2

Elastic and absorption cross sections for electron scattering by ethylene in the intermediate energy range

L M Brescansin[1], P Rawat[2], I Iga[2], M G P Homem[3,4], M-T Lee[2] and L E Machado[3]

[1] Instituto de Física 'Gleb Wataghin', UNICAMP, 13083-970 Campinas, SP, Brazil
[2] Departamento de Química, UFSCar, 13565-905 São Carlos, SP, Brazil
[3] Departamento de Física, UFSCar, 13565-905 São Carlos, SP, Brazil
[4] Laboratório Nacional de Luz Sincrotron, 13084-971, Campinas, SP, Brazil

Received 26 September 2003
Published 17 December 2003
Online at stacks.iop.org/JPhysB/37/471 (DOI: 10.1088/0953-4075/37/2/014)

Abstract

In this work, we present a joint theoretical and experimental study on electron scattering by C_2H_4 in the intermediate energy range. Calculated elastic differential, integral, and momentum-transfer as well as total (elastic + inelastic) and absorption cross sections are reported at impact energies ranging from 10 to 500 eV. Also, experimental absolute elastic cross sections are reported in the 100–500 eV range. The measurements were performed using a crossed electron beam–molecular beam geometry. The angular distributions of the scattered electrons were converted to absolute cross sections using the relative flow technique. Theoretically, a complex optical potential was used to represent the electron–molecule interaction dynamics. The Schwinger variational iterative method combined with the distorted-wave approximation was used to solve the scattering equations. The comparison between our calculated and measured results, as well as with other experimental and theoretical data available in the literature, is encouraging.

1. Introduction

Simple hydrocarbon molecules have been attracting a considerable amount of attention in the past few years, as prototype polyatomic molecules. Electron-impact cross sections for these molecules are important for understanding and modelling plasmas [1] where such molecules are produced through proton-induced chemical sputtering of graphite tiles used for walls of tokamak fusion devices. However, these data are also important for elucidating some mechanisms of astrophysical phenomena [2] and controlling plasma processing in industry [3]. For ethylene, however, although a few recent experimental data on elastic scattering are now available, much less attention has been given as yet. Experimentally, most studies to date have been concerned with measurements of total (elastic + inelastic) cross sections (TCS). In 1985, Floeder *et al* [4] measured TCS for e^-–C_2H_4 scattering between 5 and 400 eV in a transmission

experiment. TCS for C_2H_4 and C_2H_6 in the 1–400 eV range were also measured by Sueoka and Mori [5] using a retarding potential time-of-flight (RP-TOF) method and by Nishimura and Tawara [6] for energies from 4 to 500 eV, also using a linear transmission technique. Recently, TCS were also reported by Ariyasinghe and Powers [7] for the 200–1400 eV range.

Measurements of elastic differential cross sections (DCS) were carried out by Mapstone and Newell in 1992 [8] for incident energies from 3 to 15 eV and for scattering angles from 30° to 140°. Lunt *et al* [9] also studied low-energy elastic e^-–C_2H_4 scattering using two different synchrotron radiation photoionization spectrometers, focusing attention on the energy range below 2 eV. Very recently, Panajotovic *et al* [10] reported measured absolute elastic DCS, integral (ICS) and momentum-transfer cross sections (MTCS) for incident energies ranging from 1 to 100 eV using two different crossed beam spectrometers. There is a lack of measured absolute elastic cross sections for energies above 100 eV.

From the theoretical point of view, the studies on e^-–C_2H_4 scattering are equally sparse. Only a few calculations of electron scattering by this molecule have so far been reported in the literature: Schneider *et al* [11] used the complex Kohn variational method to calculate partial ICS for $^2B_{2g}$ and ^2A_g symmetries at energies below 5.5 eV. Elastic DCS, calculated within the static-exchange (SE) approximation, from 5 to 30 eV were reported by Winstead *et al* [12] using the Schwinger multichannel method (SMC). Also, in 1998 our group [13] reported elastic DCS, ICS, and MTCS for electron scattering by C_2H_4 within the static-exchange plus correlation–polarization (SECP) approximation for energies ranging from 1 to 50 eV using the iterative Schwinger variational method (SVIM) [14]. To our knowledge, no theoretical elastic DCS have ever been reported in the literature for incident energies above 50 eV.

In this paper we perform a joint theoretical and experimental study of electron scattering by C_2H_4 in the intermediate energy range. Calculated DCS, ICS, MTCS, as well as TCS and total absorption cross sections (TACS) are reported for incident energies ranging from 10 to 500 eV. Measured absolute DCS, ICS, and MTCS in the 100–500 eV range are also reported.

Our experimental elastic DCS are determined using the relative flow technique (RFT) [15–23]. Theoretically, a complex optical potential, derived from a fully molecular near-Hartree–Fock self-consistent-field (SCF) wavefunction, is used to describe the electron–molecule interaction. Here we are interested in the intermediate energy region, where absorption effects are known to be important. Indeed, almost all inelastic channels (rotational, vibrational and electronic excitations, ionization, etc) are open, thus resulting in a reduction of the flux corresponding to the elastic channel. In this energy range, conventional close-coupling calculations of electron–molecule scattering would be an arduous computational task. Therefore, the use of model absorption potentials seems to be at present the only practical manner for treating electron–atom and electron–molecule collisions in this energy range. Several model absorption potentials have been proposed and used [24], but version 3 of the quasifree-scattering model (QFSM) proposed by Staszewska *et al* [25] has been shown to yield cross sections in better agreement when compared with experiments. We have chosen this model to account for the absorption component of the electron–molecule interaction potential.

The organization of this paper is as follows. In section 2, the theory is briefly described and some details of the calculations are given and in section 3 some experimental details are briefly presented. Finally, our calculated results are compared with the present experimental and other existing theoretical and/or experimental data in section 4, where we also summarize some conclusions.

2. Theory and calculation

In the present study, a combination of the SVIM and the distorted-wave approximation (DWA) is used to solve the scattering equations. Since the details of these methods have already been

presented in previous works [14, 26], they will be only briefly outlined here. After carrying out the averaging over the molecular orientations, the laboratory-frame (LF) DCS for elastic e^-–C_2H_4 scattering is given by

$$\frac{d\sigma}{d\Omega} = \sum_L A_L(k) P_L(\cos\theta) \tag{1}$$

where θ is the scattering angle. The coefficients $A_L(k)$ in equation (1) are given by the formula

$$\begin{aligned} A_L(k) = \frac{1}{2}\frac{1}{2L+1} \sum_{\substack{p\mu l h l' h' m m' \\ p_1\mu_1 l_1 h_1 l_1' h_1' m_1 m_1'}} & (-1)^{m'-m}\sqrt{(2l+1)(2l_1+1)} \\ & \times b^{p_1\mu_1}_{l_1' h_1' m_1'} b^{p_1\mu_1{}^*}_{l_1 h_1 m_1} b^{p\mu^*}_{l' h' m'} b^{p\mu}_{lhm} a^{p_1\mu_1^*}_{l_1 h_1, l_1' h_1'}(k) a^{p\mu}_{lh,l'h'}(k) \\ & \times (l_1 0 l 0|L0)(l_1' 0 l' 0|L0)(l_1 - m_1 l m|L - M)(l_1' m_1' l' m'|LM) \end{aligned} \tag{2}$$

where $(j_1 m_1 j_2 m_2|j_3 m_3)$ are the usual Clebsch–Gordan coefficients and the auxiliary amplitudes $a^{p\mu}_{lh,l'h'}(k)$ are defined as

$$a^{p\mu}_{lh,l'h'}(k) = -\frac{\sqrt{\pi^3}}{k} i^{l'-l}\sqrt{2l'+1}\, T^{p\mu}_{k,lh;l'h'}. \tag{3}$$

The coefficients $b^{p\mu}_{lhm}$ satisfy important orthogonality conditions and are tabulated for the C_{2v} and O_h groups by Burke *et al* [27]. In equations (1)–(3), p is an irreducible representation (IR) of the molecular point group, μ is a component of this representation and h distinguishes between different bases of the same IR corresponding to the same value of l, and $T^{p\mu}_{k,lh;l'h'}$ is a partial-wave component of the elastic transition T-matrix defined as

$$T = \langle \Phi_f | V_{opt} | \Psi_i^+ \rangle, \tag{4}$$

where V_{opt} is a complex optical potential that describes the e^-–C_2H_4 interaction dynamics and is given by

$$V_{opt} = V^{SECP} + iV_{ab}. \tag{5}$$

In equation (5) V^{SECP} is the real part of the interaction potential composed of the static, the exchange, and the correlation–polarization contributions:

$$V^{SECP} = V_{st} + V_{ex} + V_{cp}, \tag{6}$$

and V_{ab} is the absorption potential. In our calculation, V_{st} and V_{ex} are derived exactly from the molecular wavefunction, whereas V_{cp} is obtained following the prescription of Padial and Norcross [28], where a short-range correlation potential between the scattering and the target electrons is defined in an inner interaction region and a long-range polarization potential in an outer region. The correlation potential is calculated by using a free-electron-gas model, derived using the target electronic density according to equation (9) of Padial and Norcross [28]. In addition, an asymptotic form of the polarization potential is used for the long-range electron–target interaction.

The absorption potential V_{ab} is that of the QFSM version 3 of Staszewska *et al* [25], given by

$$V_{ab}(\vec{r}) = -\rho(\vec{r})\left(\frac{T_L}{2}\right)^{1/2}\left(\frac{8\pi}{5k^2}k_F^3\right) H(\alpha + \beta - k_F^2)(A + B + C), \tag{7}$$

where

$$T_L = k^2 - V^{SEP}, \tag{8}$$

$$A = \frac{5k_F^3}{(\alpha - k_F^2)}, \tag{9}$$

$$B = -\frac{k_F^3(5(k^2 - \beta) + 2k_F^2)}{(k^2 - \beta)^2}, \tag{10}$$

and

$$C = 2H(\alpha + \beta - k^2)\frac{(\alpha + \beta - k^2)^{5/2}}{(k^2 - \beta)^2}. \tag{11}$$

In equations (7)–(11), k^2 is the energy (in Rydbergs) of the incident electron, k_F the Fermi momentum, and $\rho(\vec{r})$ the local electronic density of the target. $H(x)$ is a Heaviside function defined by $H(x) = 1$ for $x \geqslant 0$ and $H(x) = 0$ for $x < 0$. According to Staszewska *et al* [25],

$$\alpha(\vec{r}, E) = k_F^2 + 2(2\Delta - I) - V^{\mathrm{SEP}} \tag{12}$$

and

$$\beta(\vec{r}, E) = k_F^2 + 2(I - \Delta) - V^{\mathrm{SEP}}, \tag{13}$$

where Δ is the average excitation energy and I is the ionization potential.

The Lippmann–Schwinger scattering equation for elastic e^-–C_2H_4 collision is solved using the SVIM. In principle, this equation should be solved with the full complex optical interaction potential. Nevertheless, a tremendous computational effort would be required, particularly due to the large number of coupled equations involved, which makes such calculations practically prohibitive. On the other hand, our calculation has revealed that the magnitude of the imaginary part (absorption) of the optical potential is considerably smaller than its real counterpart. Therefore, in the present study, the scattering equations are solved using the SVIM considering only the real part of the optical potential. In SVIM calculations, the continuum wavefunctions are single-centre expanded as

$$\chi_{\vec{k}}^{\pm}(\vec{r}) = \left[\frac{2}{\pi}\right]^{1/2} \sum_{lm} \frac{(\mathrm{i})^l}{k} \chi_{klm}^{\pm}(\vec{r}) Y_{lm}(\hat{k}), \tag{14}$$

where the superscripts (+) and (−) denote the incoming-wave and outgoing-wave boundary conditions, respectively. Furthermore, the absorption part of the T matrix is calculated via DWA as

$$T_{\mathrm{ab}} = \mathrm{i}\langle \chi_{\mathrm{f}}^- | V_{\mathrm{ab}} | \chi_{\mathrm{i}}^+ \rangle, \tag{15}$$

where χ_{f}^- and χ_{i}^+ are distorted wavefunctions calculated in the SVIM. Additionally, the TCS are calculated by using the optical theorem [29].

The SCF wavefunction for the ground state was obtained using the contracted Gaussian basis set of [13]. It consists of the contracted set of Dunning [30] augmented with some uncontracted functions on the nuclei and on the centre of mass of the molecule. At the experimental equilibrium geometry of $R_{(\mathrm{C-C})} = 2.5133$ au, $R_{(\mathrm{C-H})} = 2.0333$ au, and $\theta_{(\mathrm{H-C-H})} = 116.6°$, this basis set gives an SCF energy of −78.060 60 au. This value compares well with the near-Hartree–Fock limit of −78.0616 au [31]. The dipole polarizabilities used in the calculation of the correction to the SE potential are derived from the experimental values published in [32]: $\alpha_{00} = 28.4667$, $\alpha_{20} = 7.923$ and $\alpha_{22} = 0.2625$. In the present calculation, the cut-off parameter used in the expansions of the target bound orbitals and of the SECP potential is $l_c = 24$. In SVIM calculations, all partial-wave expansions were truncated at $l_c = 16$ and 24, for incident energies below and above 20 eV, respectively, and all possible

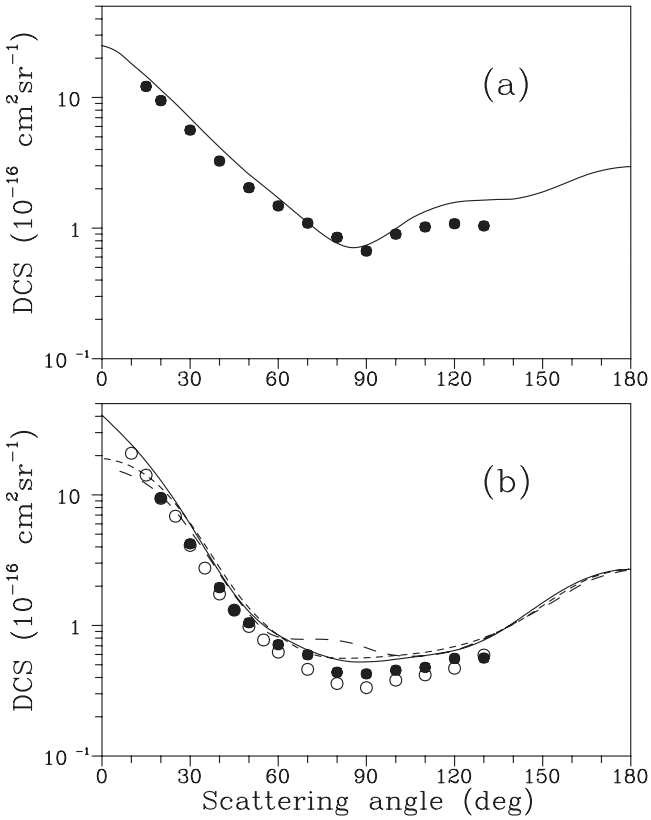

Figure 1. DCS for e^-–C_2H_4 scattering at incident energies of (a) 10 eV and (b) 20 eV. Solid curve: present calculated results; short-dashed curve: SMC results of Winstead and McKoy [40]; dashed curve: Kohn variational results of Rescigno [41]; full circles: experimental results of Panajotovic *et al* (Sophia group) [10]; open circles: experimental results of Panajotovic *et al* (ANU group) [10].

values of $h \leqslant l$ were retained. Additional terms which account for the contributions of angular momenta higher than l_c are included in the scattering amplitude calculation as follows:

$$f(\hat{k}', \hat{k}'_0) = \sum_{l,h,l',h'}^{l_c,l'_c} f_{l,h,l',h'} + f^{(\text{higher})}, \tag{16}$$

where

$$f^{(\text{higher})} = \frac{1}{2ik} \sum_{l=l_c+1}^{l_{\max}} (2l+1)(e^{2i\delta_l} - 1) P_l(\cos\theta) \tag{17}$$

and δ_l is the partial-wave phase shift, given by a closed formula:

$$\tan\delta_l = -\frac{\pi k^2 \alpha_0}{(2l-1)(2l+1)(2l+3)}. \tag{18}$$

For incident energies $E_0 \geqslant 20$ eV, angular momentum phase shifts up to $l_{\max} = 200$ were used in equation (17). The values of Δ and I in equations (12) and (13) were taken as $\Delta = I = 10.5$ eV [36]. Our SVIM calculations were all converged within five iterations.

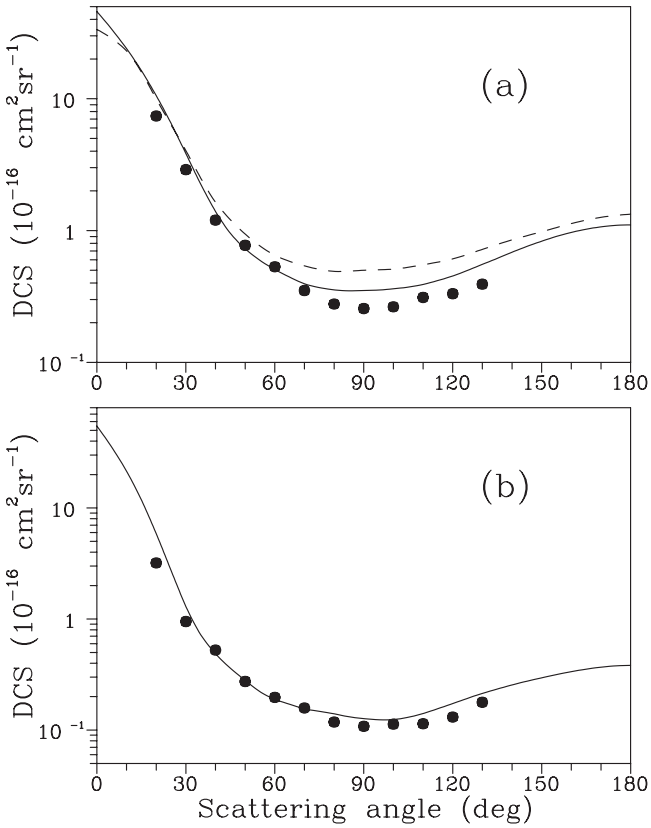

Figure 2. The same as figure 1, but for (a) 30 eV and (b) 60 eV. The symbols are the same as in figure 1, except: dashed curve: previous calculated SECP results [13].

3. Experiment

Details of our experimental set-up and procedure have already been presented elsewhere [33]. A crossed electron beam–molecular beam geometry is used to measure the relative distribution of the scattered electrons as a function of the scattering angles at a given incident electron energy. An electron beam with an estimated diameter of 1 mm is generated without any prior energy selection. The typical beam current is in hundreds of nA in the energy range covered. A molecular beam flows into the vacuum chamber via a capillary array of length $L = 5$ mm, with the individual capillary diameter $D = 0.05$ mm and an aspect ratio $\gamma = D/L = 0.01$. The scattered electrons are energy filtered by a retarding-field energy selector with a resolution of about 1.5 eV. This resolution is sufficient to distinguish electronically inelastic scattered electrons. After being energy analysed, the elastically scattered electrons are detected by a microchannel plate. During the measurements, the working pressure in the vacuum chamber is around 5×10^{-7} Torr. The recorded scattering intensities are converted into absolute elastic DCS using the RFT. Accordingly, the DCS for a gas 'x' under determination can be related to the known DCS of a secondary standard gas 'std' by

$$(\mathrm{DCS})_\mathrm{x} = (\mathrm{DCS})_\mathrm{std} \frac{I_\mathrm{x}}{I_\mathrm{std}} \frac{n_\mathrm{std}}{n_\mathrm{x}} \left(\frac{M_\mathrm{std}}{M_\mathrm{x}} \right)^{1/2}, \tag{19}$$

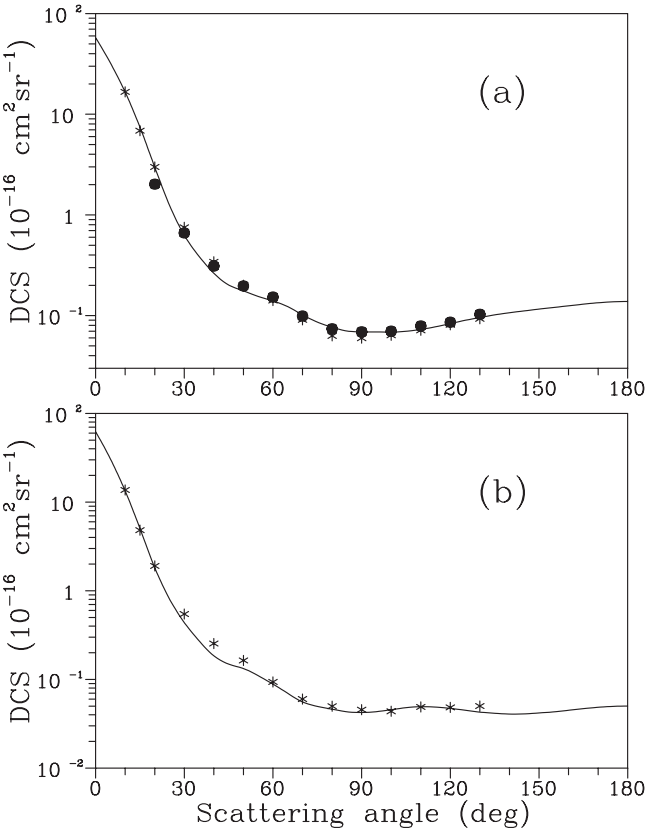

Figure 3. The same as figure 1, but for (a) 100 eV and (b) 150 eV. The symbols are the same as in figure 1, except: asterisks: present experimental results.

where I is the scattered electron intensity, n is the flow rate, and M is the molecular weight. The above equation is valid if the density distributions of the two gases, x and std, are nearly the same. This requirement is fulfilled under two conditions [34]: (i) the mean free paths λ of the two gases behind the capillaries should be equal and (ii) the Knudsen number K_L, defined as $\frac{\lambda}{L}$, must satisfy the relation $\gamma \leqslant K_L \leqslant 10$. However, several recent investigations have provided experimental evidence that even at beam flow regimes in which the K_L are significantly lower than γ, equation (19) can still be valid [21, 23]. In the present study, Ar is used as the secondary standard. The collisional diameters of Ar and C_2H_4 are 2.95 Å [35] and 4.79 Å, respectively. The latter was calculated using the van der Waals' constants reported in the *Handbook of Chemistry and Physics* [36]. Thus the theoretical pressure ratio for equal K_L will be approximately 2.65:1. The pressure behind the capillary array was taken as being 5 Torr for Ar. This corresponds to $\lambda = 16.1$ μm and $K_L = 0.0032$. In addition, the e^-–Ar absolute cross sections of Jansen *et al* [37] in the 100–500 eV energy range are used to normalize our data. Details of the analysis on experimental uncertainties have also been given elsewhere [33]. They are estimated briefly as follows. Uncertainties of random nature such as pressure fluctuations, electron beam current readings, and background scattering are estimated to be less than 2%. These contributions combined with the estimated statistical errors give an overall uncertainty of 4% in the relative DCS for each gas. Also, the experimental uncertainty associated with the normalization procedure is estimated to be 5.7%. These errors combined

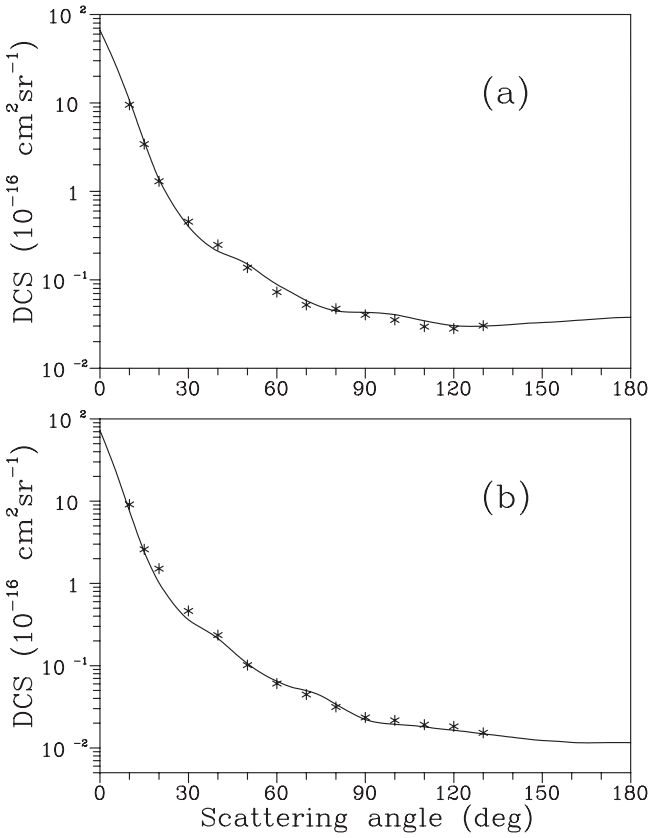

Figure 4. The same as figure 3, but for (a) 200 eV and (b) 300 eV.

with the quoted errors [37] in the absolute DCS of the secondary standard provide an overall experimental uncertainty of 11% in our absolute DCS. The absolute DCS were determined in the 10°–130° angular range. In order to obtain ICS and MTCS, an extrapolation procedure was adopted to estimate DCS at scattering angles out of that range. The extrapolation was carried out following the trend of the theoretical DCS in both forward and backward directions. The overall errors on ICS and MTCS are estimated to be 22%.

4. Results and discussion

We have selected representative results on DCS, mostly where experimental data and/or other calculations are available for comparison. The calculated DCS for e^-–C_2H_4 scattering at incident energies $E_0 = 10$, 20, 30, and 60 eV are shown in figures 1 and 2, along with the experimental results of Panajotovic *et al* [10]. At 20 eV, our DCS are also compared with the cross sections calculated using the Kohn variational technique [41] and the SMC [40]. The SMC calculation is an extension of an earlier work [12] that includes polarization effects, though treating them in a different way. Although all calculations reproduce the general features of the DCS at this energy, there are some differences between the theoretical results near the forward direction. Our model seems to reproduce the cross sections better in this angular region.

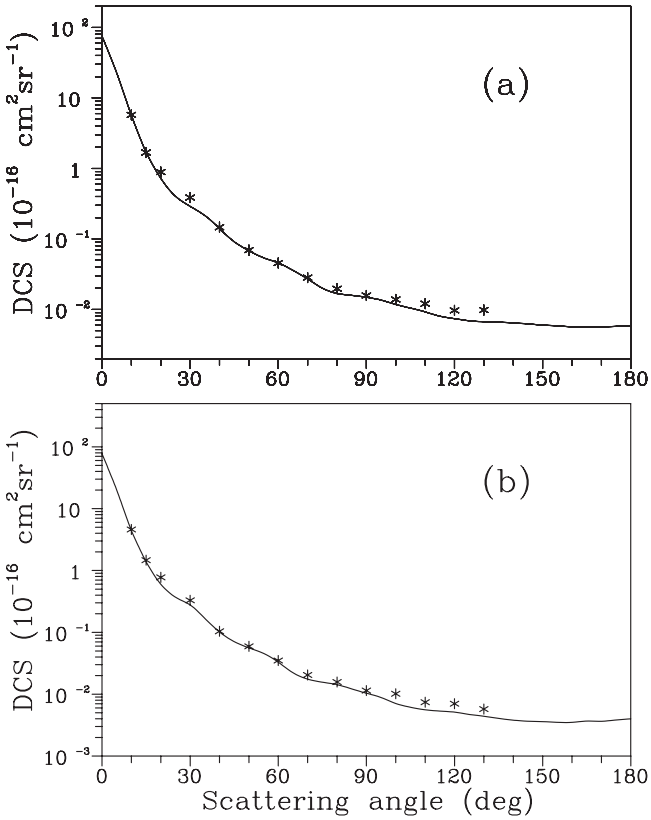

Figure 5. The same as figure 3, but for (a) 400 eV and (b) 500 eV.

When the comparison with experiments is made, it is seen that our calculated DCS are in good agreement for all incident energies considered in those figures. At 20 eV, the experimental data reveal some discrepancies between the measurements which were performed on two different experimental apparatus set-ups—however, not big enough to overshadow the good agreement of both with our theory. In particular, our calculated results are in slightly better agreement with the Sophia group's data [10]. In order to show the influence of the inclusion of the absorption potential in the cross sections, we chose a particular energy, 30 eV, for which we performed calculations without [13] and with the inclusion of that potential. As seen in figure 2(a) this influence is evident: the agreement between our calculations and the measured data is better when the absorption effects are considered.

In figures 3–5 we compare our calculated DCS with the present measured data for elastic e^-–C_2H_4 scattering in the incident energy range of 100–500 eV. The experimental data of Panajotovic *et al* (Sophia group) at 100 eV are also included. At this energy, the two sets of experimental data are in excellent agreement in the angular range where the comparison is possible. Also, our calculated results are in remarkably good agreement, both in shape and magnitude, with our measured data and with those of Panajotovic *et al* [10] in that entire energy range. The results shown in figures 1–5 support the assertion that our combined method is able to provide reliable cross sections over a very wide energy region.

Figures 6(a) and (b) show our calculated ICS and MTCS in the 10–500 eV energy range, respectively, as a function of the incident energy, along with the present experimental results and

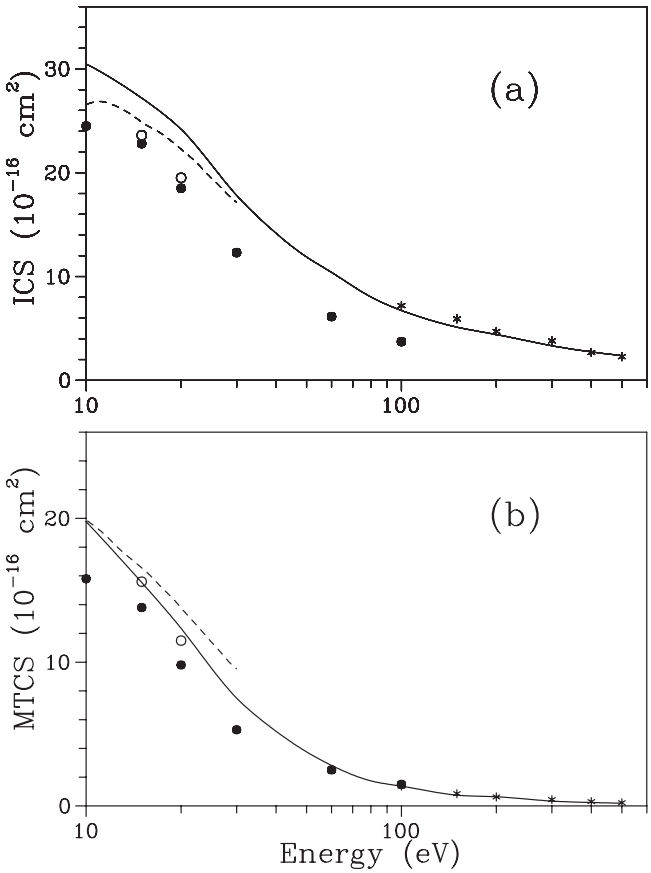

Figure 6. (a) ICS and (b) MTCS, for e^-–C_2H_4 scattering. The symbols are the same as in figures 1 and 3.

those of Panajotovic *et al* [10]. The theoretical ICS and MTCS of Winstead and McKoy [40] in the 10–30 eV range are also included for comparison. The experimental ICS below 100 eV are consistently smaller than the calculated cross sections. It is interesting to notice that at 100 eV the present measured ICS is almost a factor of two higher than the result of the Sophia group, despite the excellent agreement of their DCS with ours. This discrepancy is probably due to the different procedures of extrapolation towards the forward direction that were adopted by the experimental groups. In an extrapolation procedure, the ICS are very sensitive to the trend of the DCS in the forward direction. As the DCS at this energy are strongly enhanced in this angular region, we believe that the present experimental ICS would be more reliable, as our DCS were measured starting from 10°, whereas theirs were measured starting from 20°. Above 100 eV, however, the agreement between our experimental ICS and our calculated cross sections is very good. On the other hand, our calculated MTCS show a very good quantitative agreement with all measured data. For completeness, our measured DCS, ICS, and MTCS are also shown in table 1.

The calculated TCS and TACS are shown in figures 7(a) and (b), respectively, along with the experimental TCS of Floeder *et al* [4], Sueoka and Mori [5], Nishimura and Tawara [6], Ariyasinghe and Powers [7], and the theoretical results of Jiang *et al* [39]. Although the present

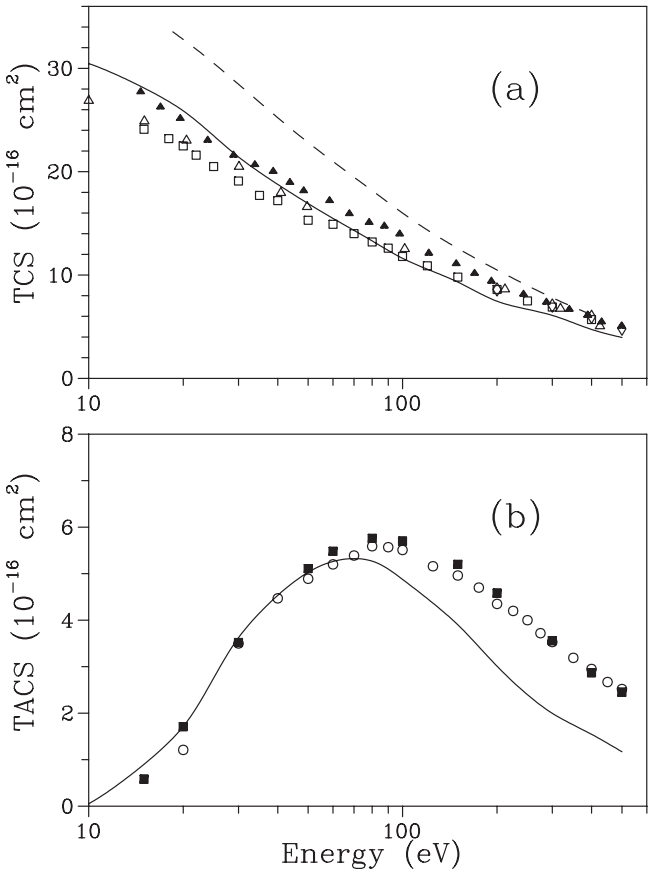

Figure 7. (a) TCS and (b) TACS for e^-–C_2H_4 scattering. The symbols are the same as in figure 3, except: dashed curve: calculated results of Jiang *et al* [39]; open squares: measured TCS of Sueoka and Mori [5]; open diamonds: experimental TCS of Ariyasinghe and Powers [7]; open triangles: experimental data of Floeder *et al* [4]; full triangles: measured TCS of Nishimura and Tawara [6]; full squares: experimental TICS of Nishimura and Tawara [38]; open circles: experimental TICS of Tian and Vidal [43].

study is unable to provide directly electron-impact total ionization cross sections (TICS) for e^-–C_2H_4, the difference between the calculated TCS and ICS provides an estimate of the TACS, which account for all inelastic contributions including both excitation and ionization processes. Nevertheless, Joshipura *et al* [42] have observed that for a set of molecules the ionization dominates the inelastic processes, the values of the TICS being about 80% of the TACS at energies around 100 eV and about 100% for energies above 300 eV. Therefore, a comparison of the present calculated TACS with experimental and calculated TICS is meaningful and would provide insight into the electron-impact ionization dynamics of this molecule. In this sense, in figure 7(b) we compare our calculated TACS with the experimental TICS of Nishimura and Tawara [38] and of Tian and Vidal [43]. Our TCS are in good agreement with at least one set of experimental results, for incident energies below 100 eV. Above this energy, our calculated TCS are slightly smaller than all the experimental values. Also, our calculated TACS show a very good qualitative agreement with the measured TICS [38, 43]. Quantitatively, for energies below 100 eV, our TACS also reproduce well the experimental TICS. Above

Table 1. Experimental DCS, ICS, and MTCS (in 10^{-16} cm^2) for elastic e^-–C_2H_4 scattering.

Angle (deg)	E_0 (eV)					
	100	150	200	300	400	500
10	1.69(1)[a]	1.37(1)	9.53(0)	9.13(0)	5.76(0)	4.60(0)
15	6.87(0)	4.83(0)	3.42(0)	2.60(0)	1.68(0)	1.47(0)
20	2.99(0)	1.91(0)	1.30(0)	1.15(0)	8.89(−1)	7.75(−1)
30	7.53(−1)	5.47(−1)	4.54(−1)	4.64(−1)	3.86(−1)	3.29(−1)
40	3.42(−1)	2.54(−1)	2.48(−1)	2.36(−1)	1.47(−1)	1.04(−1)
50	2.00(−1)	1.64(−1)	1.37(−1)	1.02(−1)	6.94(−2)	5.95(−2)
60	1.41(−1)	9.37(−2)	7.26(−2)	6.06(−2)	4.55(−2)	3.50(−2)
70	9.08(−2)	6.02(−2)	5.20(−2)	4.46(−2)	2.83(−2)	2.05(−2)
80	6.29(−2)	4.99(−2)	4.70(−2)	3.15(−2)	1.97(−2)	1.57(−2)
90	5.96(−2)	4.56(−2)	4.02(−2)	2.35(−2)	1.57(−2)	1.15(−2)
100	6.38(−2)	4.38(−2)	3.52(−2)	2.16(−2)	1.38(−2)	1.02(−2)
110	7.14(−2)	4.90(−2)	2.96(−2)	1.92(−2)	1.20(−2)	7.41(−3)
120	8.10(−2)	4.85(−2)	2.80(−2)	1.83(−2)	9.68(−3)	7.02(−3)
130	9.303(−2)	5.01(−2)	3.03(−2)	1.53(−1)	9.79(−3)	5.74(−3)
ICS	7.19(0)	5.92(0)	4.71(0)	3.80(0)	2.68(0)	2.28(0)
MTCS	1.37(0)	8.49(−1)	6.21(−1)	4.34(−1)	2.96(−1)	2.23(−1)

[a] 1.69(1) means 1.69×10^1.

this energy, our calculations underestimate the TICS, this observation being consistent with the discrepancy in the TCS between theory and experiments in the same energy range (see figure 7(a)). Actually, in both cases, the theoretical results are roughly 1–1.5 Å^2 lower than the corresponding experimental data, which seems to indicate that they have the same physical origin.

In other words, although our calculation scheme is capable of providing reliable DCS and ICS over a wide energy range, it seems to underestimate the inelastic contributions to the collisional dynamics in the intermediate energy range. This behaviour has also been systematically observed for other molecular targets [44, 45], the discrepancy being probably due to the model absorption potential that we used in our calculations. Investigations using several recently proposed model potentials [46–48] are under way.

Acknowledgments

This research was partially supported by the Brazilian agencies CNPq, FINEP-PADCT, CAPES and FAPESP.

References

[1] Janev R K 1993 *Atomic and Plasma–Material Interaction Processes in Controlled Thermonuclear Fusion* ed R K Janev and H W Drawin (Amsterdam: Elsevier) p 27
[2] Perry J J, Kim Y H, Fox J L and Porter H S 1999 *J. Geophys. Res.* **104** 16541
[3] Morgan W L 2000 *Adv. At. Mol. Opt. Phys.* **43** 79
[4] Floeder K, Fromme D, Raith W, Schwab A and Sinapius G 1985 *J. Phys. B: At. Mol. Phys.* **18** 3347
[5] Sueoka O and Mori S 1986 *J. Phys. B: At. Mol. Phys.* **19** 4035
[6] Nishimura H and Tawara H 1991 *J. Phys. B: At. Mol. Opt. Phys.* **24** L363
[7] Ariyasinghe W M and Powers D 2002 *Phys. Rev.* A **66** 052716
[8] Mapstone B and Newell W R 1992 *J. Phys. B: At. Mol. Opt. Phys.* **25** 491
[9] Lunt S L, Randell J, Ziesel J P, Mrotzek G and Field D 1994 *J. Phys. B: At. Mol. Opt. Phys.* **27** 1407

[10] Panajotovic R, Kitajima M, Tanaka H, Jelisavcic M, Lower J, Campbell L, Brunger M J and Buckman S 2003 *J. Phys. B: At. Mol. Opt. Phys.* **36** 1615
[11] Schneider B I, Rescigno T N, Lengsfield B H III and McCurdy C W 1991 *Phys. Rev. Lett.* **66** 2728
[12] Winstead C, Hipes P G, Lima M A P and McKoy V 1991 *J. Chem. Phys.* **94** 5455
[13] Brescansin L M, Machado L E and Lee M T 1998 *Phys. Rev.* A **57** 3504
[14] Lucchese R R, Raseev G and McKoy V 1982 *Phys. Rev.* A **25** 2572
[15] Srivastava S K, Chutjian A and Trajmar S 1975 *J. Chem. Phys.* **63** 2659
[16] Brinkman R T and Trajmar S 1981 *J. Phys. E: Sci. Instrum.* **14** 245
[17] Khakoo M A and Trajmar S 1986 *Phys. Rev.* A **34** 138
[18] Nickel J C, Zetner P W, Shen G and Trajmar S 1989 *J. Phys. E: Sci. Instrum.* **22** 730
[19] Brunger M J, Buckman S J, Newman D J and Alle D T 1991 *J. Phys. B: At. Mol. Opt. Phys.* **24** 1435
[20] Alle D T, Gulley R J, Buckman S J and Brunger M J 1992 *J. Phys. B: At. Mol. Opt. Phys.* **25** 1533
[21] Buckman S J, Gulley R J, Moghbelalhossein M and Bennett S J 1993 *Meas. Sci. Technol.* **4** 1143
[22] Khakoo M A, Jayawera T, Wang S and Trajmar S 1993 *J. Phys. B: At. Mol. Opt. Phys.* **26** 4845
[23] Tanaka H, Ishikawa T, Masai T, Sagara T, Boesten L, Takekawa M, Itikawa Y and Kimura M 1998 *Phys. Rev.* A **57** 1798
[24] Lee M T, Iga I, Machado L E and Brescansin L M 2000 *Phys. Rev.* A **62** 062710
[25] Staszewska G, Schwenke D W and Truhlar D G 1984 *Phys. Rev.* A **29** 3078
[26] Lee M T and McKoy V 1983 *Phys. Rev.* A **28** 697
[27] Burke P G, Chandra N and Gianturco F A 1972 *J. Phys. B: At. Mol. Phys.* **5** 2212
[28] Padial N T and Norcross D W 1984 *Phys. Rev.* A **29** 1742
[29] Joachain C J 1983 *Quantum Collision Theory* (Amsterdam: North-Holland)
[30] Dunning T H Jr 1970 *J. Chem. Phys.* **53** 2823
[31] Clementi E and Popkic H 1972 *J. Chem. Phys.* **57** 4870
[32] Hills G W and Jones W J 1975 *J. Chem. Soc. Faraday Trans.* II **71** 812
[33] Iga I, Lee M T, Homem M G P, Machado L E and Brescansin L M 2000 *Phys. Rev.* A **61** 227081
[34] Olander D R and Kruger V 1970 *J. Appl. Phys.* **41** 2769
[35] Roth A 1982 *Vacuum Technology* (Amsterdam: North-Holland)
[36] Lide D V (ed) 1993 *Handbook of Chemistry and Physics* 73rd edn (Boca Raton, FL: CRC Press)
[37] Jansen R H J, de Heer F J, Luyken H J, van Wingerden B and Laauw H J B 1976 *J. Phys. B: At. Mol. Phys.* **9** 185
[38] Nishimura H and Tawara H 1994 *J. Phys. B: At. Mol. Opt. Phys.* **278** 2063
[39] Jiang Y, Sun J and Wan L 1997 *J. Phys. B: At. Mol. Opt. Phys.* **30** 5025
[40] Winstead C and McKoy V 2002 as quoted by [10]
[41] Rescigno T 2002 as quoted by [10]
[42] Joshipura K N, Vinodkumar M and Patel U M 2001 *J. Phys. B: At. Mol. Opt. Phys.* **34** 509
[43] Tian C and Vidal C R 1998 *Chem. Phys. Lett.* **288** 499
[44] Lee M T, Iga I, Homem M G P, Brescansin L M and Machado L E 2002 *Phys. Rev.* A **65** 062702
[45] Lee M T, Iga I, Machado L E and Brescansin L M 2000 *Phys. Rev.* A **62** 062710
[46] Neugebauer J, Reiher M and Hinze J 2002 *Phys. Rev.* A **66** 022717
[47] Salvat F 2003 *Phys. Rev.* A **68** 012708
[48] Blanco F and García G 2003 *Phys. Rev.* A **67** 022701